

**C. Stephan, G. Pennisi**  
(ONERA)

**G. Michon**  
University of Toulouse  
(ICA, CNRS, ISAE)

E-mail: cyrille.stephan@onera.fr

DOI: 10.12762/2018.AL14-08

## Vibration Mitigation Based on Nonlinear Absorbers

The design of vibration absorbers is a challenging task for complex real-life structures. Although several technological solutions have now reached maturity, a need for better efficiency in terms of added mass, broadband frequency range and level of reduction requires the study of new ideas and concepts coming from nonlinear dynamics. In this paper an introduction to a class of absorbers called Nonlinear Energy Sinks (NES) is proposed to highlight their potential for vibration mitigation. After a reminder of the different categories of vibration control, some principles of NES and their relationship with linear absorbers are presented. Two experimental NES prototypes are studied and the results have shown interesting capacities for vibration mitigation.

### Introduction

During their operation, aeronautical structures often endure strong dynamical excitations and their vibrations can reach high levels. This has many undesirable consequences: shorter lifetime of structures, less user comfort in terms of the vibrations felt (and even vibroacoustics), and penalized controllability of trajectories (aircraft, missiles). For all of these reasons, the study of technological solutions that can mitigate vibrations is still an active and open research subject.

Indeed, several ways have already been investigated and the mitigation methods can be classified into three main categories.

- Active control methods have been widely developed over the last decades [1]. The principle is to reduce undesirable vibrations by generating an out-of-phase input. Active control usually gives good performance in terms of vibration reduction, but it requires an external energy supply. Since adding excitation to structures, even for their benefit, could seem tricky and perilous, active control has not achieved great success in industrial applications.
- Semi-active control methods using electro- and magneto-rheological fluids have been proposed [6], [1]. The particularity of these fluids lies in their varying viscosity with respect to the electric or magnetic field in which they are immersed. Since no energy is transferred to the controlled system, these techniques are robust and reliable, while offering a vibration reduction level similar to that of active techniques. However, both the modeling of fluid behaviors and the development of the controller represent major challenges that still complicate the use of the systems for real-life structures.
- Passive control methods reduce vibrations by adding to the structure a dissipative material [16] or a Dynamical Vibration Absorber (DVA) [1], [5]. Given that this can be achieved by

using only mechanical components, this technique is an important alternative to the previous methods. DVAs can behave linearly or nonlinearly, with the latter case being the main subject of this article.

Indeed, nonlinear absorbers, also called NES (Nonlinear Energy Sinks), have drawn the attention of many laboratories in recent years, since their performance and robustness are very promising. However, relying on nonlinear dynamics for vibration mitigation is also very challenging, because almost all concepts coming from linear dynamics no longer apply for these devices. In this paper, we aim to present the basic principles of NES and their potential for industry. In a first part, we will introduce the concept of NES and its link to linear absorbers. The second part will be devoted to two experimental NES prototypes developed in our facilities.

### Reminder of the concept of linear absorbers

Before presenting nonlinear absorbers, a reminder of the linear version should be instructive, since it preceded them historically. The Tuned Mass Damper (TMD) is probably the most popular device for passive vibration mitigation of mechanical structures. Thanks to its linear behavior and the well-established mathematical theory that it relies on, the TMD is widely implemented in various areas, such as civil buildings (e.g. Millennium Bridge, Taipei 101 skyscraper, Burj-el-Arab Hotel), electromechanical engineering structures (cars and high-tension lines), and aircraft (especially helicopters). Despite being widely used in industrial applications, the design of such absorbers can still be a challenging problem when it is coupled to complex structures.

In 1911, Frahm initiated the TMD with a patent describing his ideas. He considered a small mass  $m_2$  coupled to a linear oscillator (LO) by a linear spring  $k_2$ . In his works, the LO is itself made of a mass  $m_1$  and a linear spring  $k_1$ , the LO is forced by a harmonic excitation, and damping terms are skipped in computations. If the natural angular frequencies of both masses  $\omega_1$  and  $\omega_2$  are set to be equal, then it can be shown that the movement of a large mass is minimized when the LO is excited at its natural frequency. Hence, designing a TMD is basically tuning the eigenfrequency of a small mass to the critical frequency of a structure.

Considering damping terms  $c_1$  and  $c_2$  complicates the reasoning. Ormondroyd and Den Hartog [17] first proposed a damped version of the absorber by adding  $c_2$  to the design parameters. An optimization process is then undertaken by means, for example, of the  $H_\infty$  technique or, more commonly now, the Den Hartog method, called the fixed-point theory [5].

Unfortunately, when the damping term  $c_1$  of the LO is also taken into account, the fixed-point theory can no longer be used. Nevertheless, several solutions have been proposed, based on the Chebyshev min-max criterion [18], control theory [24] [25], perturbation techniques [1] [8] and nonlinear programming [13] [14].

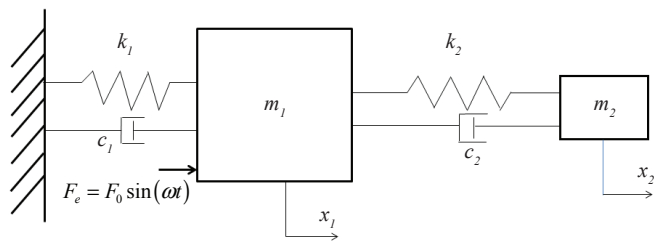


Figure 1 – A Tuned Mass Damper coupled to a linear oscillator (LO)

Although the design of TMD is now known and well mastered, it still has two main drawbacks. First, by definition, a TMD needs to be tuned to the natural frequency of an undesirable mode. Thus, its efficiency is strongly related to the actual closeness  $|\omega_2 - \omega_1|$ . However, if  $\omega_1$  is itself badly known or changing (lack of experimental testing, evolution over time, or influence of nonlinear components), the expected degree of closeness cannot be easily fulfilled, and the efficiency of the TMD drops drastically. Furthermore, since the TMD has to be tuned to one specific frequency, it is difficult, or even impossible, to damp several modes of a multiple-degree-of-freedom system with the same device.

Secondly, it can be shown that the efficiency of a TMD also depends on the mass ratio  $\varepsilon = m_2/m_1$ . In general, the order of magnitude  $\varepsilon$  is about 10%, even though lower values can be obtained for particular applications. However, it represents a significant added mass, which is highly undesirable in certain domains, such as aircraft.

## Principles of Nonlinear Absorbers

The evolution from linear to nonlinear absorbers has been driven by the need to find an answer to the two previously mentioned drawbacks of TMD: the lack of robustness and, in a less important aspect, the significant added mass. The first studies focusing on using nonlinearities in vibration mitigation date back to the 50s [22] [20] [1]. In 1982, a first practical nonlinear absorber using a softening stiffness was presented [12].

A nonlinear absorber can be outlined as a mass  $m_2$  that is coupled to a structure by a link  $F_{nl}$ . The device mass-link behaves nonlinearly as a function of its relative (or sometimes absolute) movement. In the specialized literature, the dynamical law  $F_{nl}(\cdot)$  of this link is generally called a "restoring force" [28].

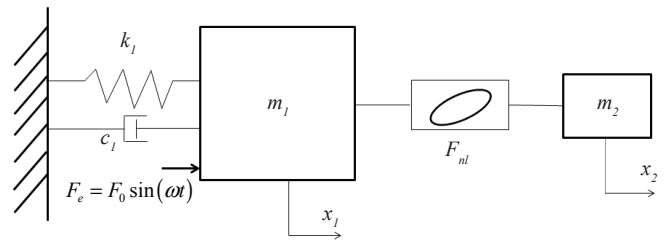


Figure 2 – A nonlinear absorber coupled to a linear oscillator

For a nonlinear absorber, the restoring force can take many forms (polynomial, friction, hysteretic, impacts, etc.), with the notable exception of the linear one. If the coefficients of the purely nonlinear part of  $F_{nl}$  are minor compared to its linear part, the restoring force can be approximated by its linear and nonlinear components

$$F_{nl}(x, \dot{x}) = kx + c\dot{x} + \text{other minor nonlinear terms} \quad [1]$$

The dynamics of the small mass  $m_2$  are then close to the behavior of a TMD, except that it depends on amplitude. In fact, it does not show solutions specific to nonlinear dynamics.

When the dynamics of the primary mass  $m_1$  are not purely linear (*i.e.*,  $k_1$  and  $c_1$  are not constant), a relevant solution consists in designing an absorber whose restoring force is tuned according to the restoring force of the primary system. Such an absorber is called a Nonlinear Tuned Vibration Absorber (NTVA) [11].

Nevertheless, let us assume now that the dynamics of the primary system are linear, and that the nonlinear part is only due to the restoring force of the absorber. When the nonlinear restoring force of  $m_2$  has no linear stiffness part, *i.e.*,  $dF_{nl}/dx = 0$ , then this DVA belongs to a specific category called "essentially nonlinear absorbers", because it cannot be approximated for small displacements by a linear spring.

Essentially, nonlinear absorbers captured the attention of researchers especially, because of their ability to "adapt" themselves to the primary system that they are attached to without being tuned to a specific frequency. Since they do not have a preferential resonant frequency, they are able to interact with the primary system over a broad range of frequencies and then to be effective on all of the modes within that range. Nonlinear Targeted Energy Transfer (TET or energy pumping) was observed by Gendelman [9], who studied a 2-DOF system composed of a linear oscillator nonlinearly coupled to an oscillator with zero linear stiffness. Not having a linear stiffness is a crucial point in order to not have a preferential frequency of oscillation. In [26] it was shown that when the energy of the LO is above a certain threshold, a localized periodic motion of the nonlinear oscillator is excited so that the energy is transferred from the LO and finally dissipated. A nonlinear absorber exhibiting this kind of behavior is called a Nonlinear Energy Sink (NES).

Furthermore, if the linear stiffness coefficient decreases further and becomes negative, there are two points of equilibrium instead of one. The resulting bi-stable absorber could be much more reactive

because the TET activation threshold is lower [15]. In any case, creating a negative linear stiffness requires more imagination, and elegant technological solutions based on magnets have been proposed in [3].

In the following sections we will present two NES prototypes: the cubic stiffness NES and the Vibro-Impact NES. For each case, the experimental and analytic study of the NES coupled to a harmonically forced Linear Oscillator (LO) will be carried out. The systems will be analyzed both analytically and experimentally. Finally, their vibratory behaviors will be explained through the analytical models.

### Experimental Case No. 1: the cubic stiffness NES

The inspiration for the first NES comes from the literature [26] [27]. The LO is composed of a moving mass of 63.2kg (see Figure 3), attached to the ground by 4 springs. The LO can translate along one direction only. Its natural frequency is 5.05 Hz. The LO is excited by one modal shaker, with a cell force between the LO and the shaker. A lighter moving mass of 0.61 kg is installed on the top of the LO: it is the NES. Through linear bearings, the NES can move along two shafts. The restoring force of the NES is generated by 4 springs that can rotate and lengthen to follow the translation of the NES (see Figure 4). The NES/ LO mass ratio is 0.97%.

A sketch of the NES displacement is given in Figure 5. We assume that the length of the springs is  $l_0$  at rest (totally free, not yet installed

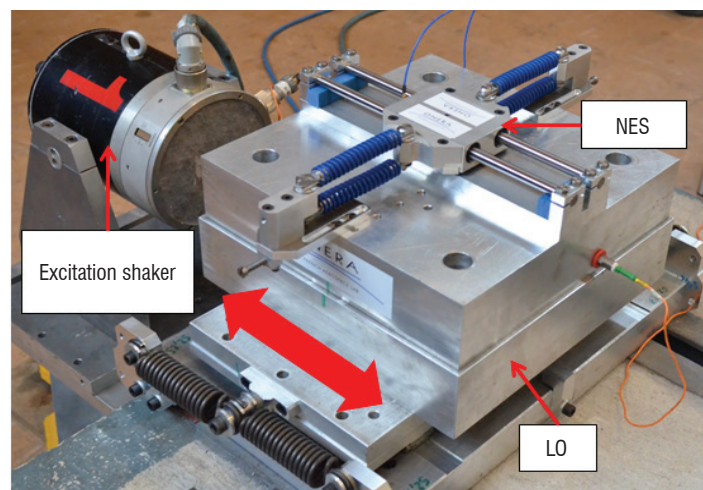


Figure 3 – A cubic stiffness NES on a LO

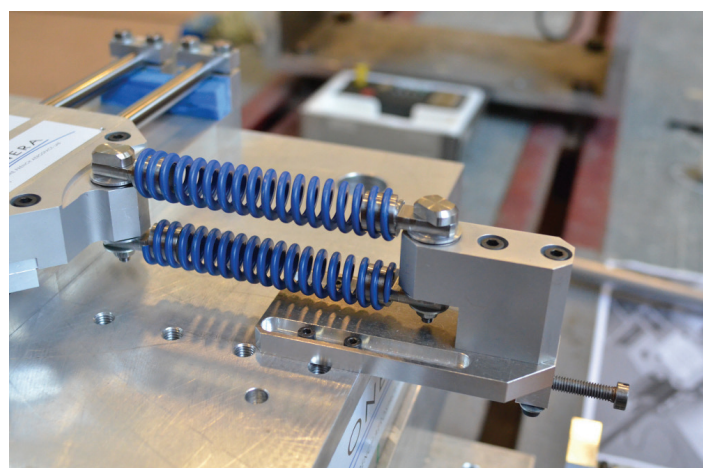


Figure 4 – The NES attached by springs to the LO

on the LO) and  $l$  when it is installed with zero-translation of the NES ( $x = 0$ ). For a translation  $x$ , its extension  $\sqrt{l^2 + x^2}$  is given by a simple geometrical projection. Thus, the restoring force is (here only the conservative part):

$$f_{nl}(x) = 2k(\sqrt{l^2 + x^2} - l) \quad [2]$$

where  $k$  is the stiffness coefficient of two parallel springs. Using a Taylor series development, the nonlinear relationship between the displacement and the restoring force can be approximated by a 3<sup>rd</sup> degree polynomial

$$f_{nl}(x) \approx k_1 x + k_3 x^3 \quad [3]$$

With the stiffness coefficients given by

$$\begin{cases} k_1 = \frac{2P}{l} + 2k\left(1 - \frac{l_0}{l}\right) \\ k_3 = \frac{kl_0}{l^3} - \frac{P}{l^3} \end{cases} \quad [4]$$

where  $P$  is the preload of two parallel springs. As can be noticed by the expression of  $k_1$ , the linear part of  $f_{nl}$  depends on the level of preload  $P$  and on the relative extension of the springs installed  $l_0/l$ . For a pure cubic restoring force,  $k_1$  set to null requires  $P = 0$  and  $l = l_0$ .

Zero-preload cannot be guaranteed by extension springs: in fact, by design, extension springs always have a certain amount of preload  $P$ . This is the reason why here compression springs were selected for the NES, even though they are used extended (see Figure 4). Given that their coils are non-contiguous, they guarantee a regular Hooke law, even for a small extension of the springs, and then have a preload  $P$  that is almost negligible.

Experiments were performed to ensure the nonlinear relationship between displacement and force. The static force is identified by blocking the movement of the LO and by attaching weights to the NES. The static displacements due to weights were successively measured by a Laser sensor (see Figure 6). The curve obtained shows the typical inverted S shape of a cubic stiffness force. Furthermore, a polynomial was curve-fitted on data and computed

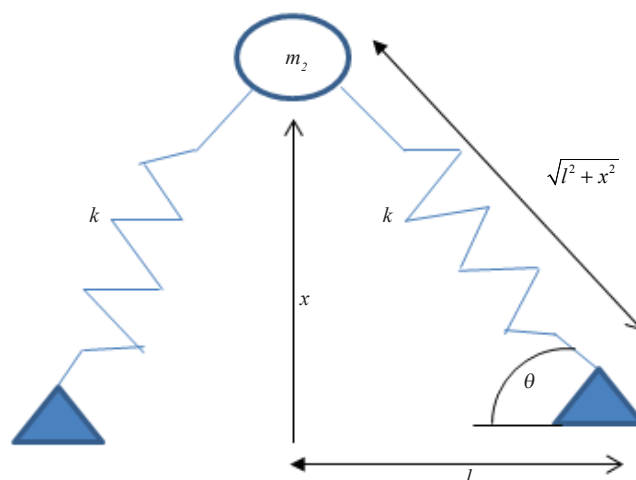


Figure 5 – Simplified movement model of the NES

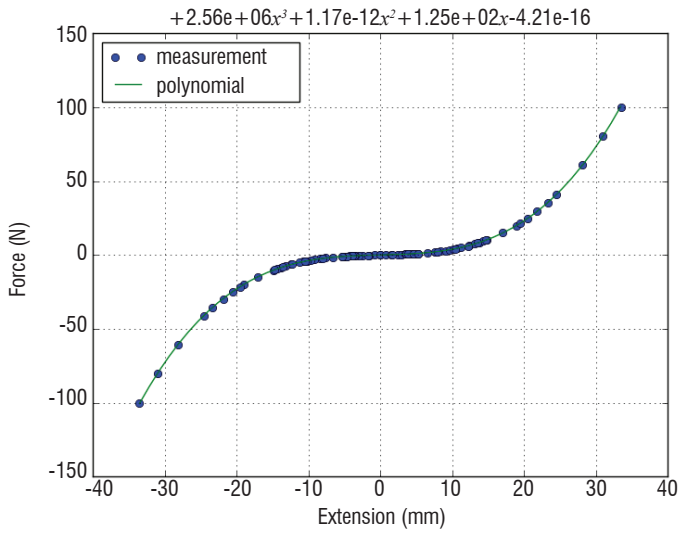


Figure 6 – Static force identified with weights

coefficients (top of Figure 6) ensuring that the cubic part is predominant over the linear part.

Finally, the restoring force  $F_{nl}$  comprises the nonlinear conservative part  $F_{nl}^c$ , which has just been derived, and a dissipative part. For the sake of simplicity, this dissipative part is modeled here by a viscous damping  $c_a \dot{x}$ . Hence, the restoring force  $F_{nl}$  is given by

$$F_{nl}(x, \dot{x}) = c_a \dot{x} + f_{nl}(x) \quad [5]$$

Hopefully, in this case, the conservative and dissipative parts are clearly distinct, making the following dynamical analysis easier. It should be noted that, in general, nonlinear oscillator equations are more complicated and formulae usually involve entangled displacement  $x$  and speed  $\dot{x}$  terms.

Dynamical equations of the coupled system (Figure 2) can now be derived by considering  $x_s$ , the displacement of the LO and  $x_a$ , the displacement of the NES.

$$\begin{cases} m_s \ddot{x}_s + c_s \dot{x}_s + k_s x_s + f_{nl}(x_s - x_a) = F_e \sin(\bar{\Omega}t) \\ m_a \ddot{x}_a + c_a (\dot{x}_a - \dot{x}_s) + f_{nl}(x_a - x_s) = 0 \end{cases} \quad [6]$$

Equations clearly show the dependency of the restoring force as a function of the relative displacement  $x_s - x_a$ . Let us now introduce the following change of variables

$$\begin{aligned} \varepsilon &= \frac{m_2}{m_1}, \omega_0^2 = \frac{k_1}{m_1}, K = \frac{k_2}{m_2 \omega_0^2}, \lambda_1 = \frac{c_1}{m_2 \omega_0}, \\ \lambda_2 &= \frac{c_2}{m_2 \omega_0}, \bar{\Omega} = \frac{\Omega}{\omega_0}, \tau = \omega_0 t, \frac{dx}{dt} = \omega_0 \dot{x}, \\ \frac{d^2x}{dt^2} &= \omega_0^2 \ddot{x}, F = \frac{F_e}{\varepsilon m_1 \omega_0^2} \end{aligned} \quad [7]$$

And the following change of coordinates

$$v = x_s + \varepsilon x_a, w = x_s - x_a \quad [8]$$

Thus, the system of dynamical equations [6] becomes

$$\begin{cases} \ddot{v} + \frac{\varepsilon}{1+\varepsilon} \lambda_1 (\dot{v} + \varepsilon \dot{w}) + \frac{1}{1+\varepsilon} (v + \varepsilon w) = \varepsilon F \sin(\Omega \tau) \\ \ddot{w} + \frac{\varepsilon}{1+\varepsilon} \lambda_1 (\dot{v} + \varepsilon \dot{w}) + \lambda_2 (1+\varepsilon) \dot{w} \\ + \frac{1}{1+\varepsilon} (v + \varepsilon w) + K(1+\varepsilon) w^3 = \varepsilon F \sin(\Omega \tau) \end{cases} \quad [9]$$

The cubic term in the second equation prevents the system from being resolved analytically. In any case, approximated periodic solutions can be sought through a combination of the Complexification-Averaging method and the Multiple Scales method [1]. First, complex variables are introduced

$$\begin{aligned} \psi_1 &= \dot{v} + i\Omega v, & \psi_2 &= \dot{w} + i\Omega w \\ \psi_1 &= \phi_1 e^{i\Omega \tau}, & \psi_2 &= \phi_2 e^{i\Omega \tau} \end{aligned} \quad [10]$$

noting that

$$\begin{aligned} v &= \frac{1}{2i\Omega} (\psi_1 - \psi_1^*), & w &= \frac{1}{2i\Omega} (\psi_2 - \psi_2^*) \\ \dot{v} &= \frac{1}{2} (\psi_1 + \psi_1^*), & \dot{w} &= \frac{1}{2} (\psi_2 + \psi_2^*) \\ \ddot{v} &= \dot{\psi}_1 - \frac{i\Omega}{2} (\psi_1 + \psi_1^*), & \ddot{w} &= \dot{\psi}_2 - \frac{i\Omega}{2} (\psi_2 + \psi_2^*) \end{aligned} \quad [11]$$

Thanks to complex variables, fast oscillations of the system at the excitation frequency  $\Omega$  can be separated from slow modulations of complex amplitudes. The following system is obtained

$$\begin{cases} \dot{\psi}_1 - \frac{i\Omega}{2} (\psi_1 + \psi_1^*) + \frac{\varepsilon}{1+\varepsilon} \lambda_1 \left[ \frac{1}{2} (\psi_1 + \psi_1^*) + \frac{\varepsilon}{2} (\psi_2 + \psi_2^*) \right] \\ + \frac{1}{2i\Omega(1+\varepsilon)} \left[ \frac{1}{2} (\psi_1 + \psi_1^*) + \frac{\varepsilon}{2} (\psi_2 + \psi_2^*) \right] = \varepsilon F \sin(\Omega \tau) \\ \dot{\psi}_2 - \frac{i\Omega}{2} (\psi_2 + \psi_2^*) + \frac{\varepsilon}{1+\varepsilon} \lambda_1 \left[ \frac{1}{2} (\psi_1 + \psi_1^*) + \frac{\varepsilon}{2} (\psi_2 + \psi_2^*) \right] \\ + 2\lambda_2 (1+\varepsilon) (\psi_2 + \psi_2^*) \\ + \frac{1}{2i\Omega(1+\varepsilon)} \left[ \frac{1}{2} (\psi_1 + \psi_1^*) + \frac{\varepsilon}{2} (\psi_2 + \psi_2^*) \right] \\ + (1+\varepsilon) \frac{iK}{8\Omega^3} (\psi_2 - \psi_2^*)^3 = \varepsilon F \sin(\Omega \tau) \end{cases} \quad [12]$$

In a second step, equations [12] are averaged over the fast scale, *i.e.*, keeping terms only of  $e^{i\Omega \tau}$ . Then, terms of  $\psi_i$  are replaced by  $\phi_i e^{i\Omega \tau}$  and, hence, equations are simplified to

$$\begin{cases} \dot{\phi}_1 + \frac{i\Omega}{2} \phi_1 + \frac{\varepsilon \lambda_1}{2(1+\varepsilon)} (\phi_1 + \varepsilon \phi_2) \\ - \frac{i}{2\Omega(1+\varepsilon)} (\phi_1 + \varepsilon \phi_2) + \frac{i\varepsilon F}{2} = 0 \\ \dot{\phi}_2 + \frac{i\Omega}{2} \phi_2 + \frac{\varepsilon \lambda_1}{2(1+\varepsilon)} (\phi_1 + \varepsilon \phi_2) - \frac{i}{2\Omega(1+\varepsilon)} (\phi_1 + \varepsilon \phi_2) \\ + \frac{\lambda_2}{2} (1+\varepsilon) \phi_2 - (1+\varepsilon) \frac{i3K_3}{8\Omega^3} |\phi_2|^2 \phi_2 + \frac{i\varepsilon F}{2} = 0 \end{cases} \quad [13]$$

It is important to remember that  $\phi_1$  and  $\phi_2$  are the slow evolutions of amplitudes for a 1:1 resonance. Thus, the temporal evolution of the

LO-NES couple is governed by the previous system of equations [13], under the assumption of a periodic movement of both oscillators at frequency  $\Omega$ .

In a third step, the method of Multiple Scales is used to obtain approximated solutions [1]. The idea is to break down the time scale  $\tau$  into several time subscales that depend on  $\tau$  and  $\varepsilon$ . Derivation is performed through a series of partial derivatives

$$\frac{d}{d\tau} = \frac{\partial}{\partial \tau_0} + \varepsilon \frac{\partial}{\partial \tau_1} + \varepsilon^2 \frac{\partial}{\partial \tau_2} + \dots, \quad \tau_k = \varepsilon^k \tau, \quad k = 0, 1, 2, \dots \quad [14]$$

Solutions  $\phi_1$  and  $\phi_2$  are written as polynomials of  $\varepsilon$

$$\begin{aligned} \phi_1 &= \phi_{10} + \varepsilon \phi_{11} + o(\varepsilon), & \frac{d\phi_1}{d\tau} &= \frac{\partial \phi_{10}}{\partial \tau_0} + \varepsilon \left( \frac{\partial \phi_{11}}{\partial \tau_0} + \frac{\partial \phi_{10}}{\partial \tau_1} \right) + o(\varepsilon) \\ \phi_2 &= \phi_{20} + \varepsilon \phi_{21} + o(\varepsilon), & \frac{d\phi_2}{d\tau} &= \frac{\partial \phi_{20}}{\partial \tau_0} + \varepsilon \left( \frac{\partial \phi_{21}}{\partial \tau_0} + \frac{\partial \phi_{20}}{\partial \tau_1} \right) + o(\varepsilon) \end{aligned} \quad [15]$$

Furthermore, the excitation frequency is assumed to be close to the natural frequency of the LO

$$\Omega = 1 + \varepsilon \sigma \quad [16]$$

where  $\sigma$  denotes a small variation around the natural frequency.

By approximating the system of dynamical equations [13] through this derivation, we can group the terms proportional to  $\varepsilon^0$ :

$$\varepsilon^0 : \begin{cases} \frac{\partial \phi_{10}}{\partial \tau_0} = 0 \\ \frac{\partial \phi_{20}}{\partial \tau_0} + \frac{\lambda_2}{2} \phi_{20} + \frac{i}{2} (\phi_{20} - \phi_{10}) - \frac{3}{8} i K |\phi_{20}|^2 \phi_{20} = 0 \end{cases} \quad [17]$$

At the first time scale  $\tau_0 = \varepsilon^0 \tau$ , amplitude modulations do not depend on the force amplitude  $F$ . In fact,  $F$  appears at the slower time scale  $\tau_1 = \varepsilon^1 \tau$ . Then, the dynamical system [17] at scale  $\tau_0$  is written in polar form

$$\phi_{10} = N_{10} e^{i\theta_{10}}, \quad \phi_{20} = N_{20} e^{i\theta_{20}} \quad [18]$$

Introducing these polar forms into the dynamic equations [17] at scale  $\varepsilon^0$ , after separating the real and complex parts, we obtain

$$\begin{cases} \frac{\partial N_{10}}{\partial \tau_0} = 0 \\ \frac{\partial N_{20}}{\partial \tau_0} = -\frac{\lambda_2}{2} N_{20} + \frac{N_{10}}{2} \sin(\theta_0) \\ \frac{\partial \theta_0}{\partial \tau_0} = \frac{N_{10}}{2N_{20}} \cos(\theta_0) - \frac{1}{2} + \frac{3}{8} K_3 N_{20}^2 \end{cases} \quad [19]$$

with  $\theta_0 = \theta_{20} - \theta_{10}$ . At equilibrium, this phase is given by

$$\begin{cases} \sin(\theta_0) = \lambda_2 \frac{N_{20}}{N_{10}} \\ \cos(\theta_0) = \frac{N_{20}}{N_{10}} \left( 1 - \frac{3}{4} K N_{20}^2 \right) \end{cases} \quad [20]$$

By squaring both expressions [20] and adding them, the fixed points of the system [19] satisfy the equation

$$(\lambda_2^2 + 1)Z - \frac{3}{2}KZ^2 + \frac{9}{16}K^2Z^3 = N_{10}^2, \quad \text{with } Z = N_{20}^2 \quad [21]$$

This equation defines the invariant manifold of the coupled system: it means that it gives a relation between the main parameters of the system that can characterize its amplitude evolution. For a fixed value of the amplitude  $N_{10}$ , this 3<sup>rd</sup> degree polynomial can be solved analytically: for each value of  $N_{10}$ , either 1 or 3 solutions can be found for  $N_{20}$ .

To know the nature of the solutions given by this invariant manifold, we need to study the eigenvalues of the stability matrix

$$M_{\varepsilon^0} = \begin{bmatrix} 0 & 0 & 0 \\ \frac{\lambda_2 N_{20}}{2N_{10}} & -\frac{\lambda_2}{2} & \frac{N_{20}}{2} \left( 1 - \frac{3}{4} K N_{20}^2 \right) \\ \frac{1}{2N_{10}} \left( 1 - \frac{3}{4} K N_{20}^2 \right) & -\frac{1}{2N_{20}} + \frac{9}{8} K N_{20} & -\frac{\lambda_2}{2} \end{bmatrix} \quad [22]$$

This matrix was computed by considering small perturbations of the previous system of dynamical equations. It can be observed that the stability matrix is independent of the phase difference  $\theta_0$ .

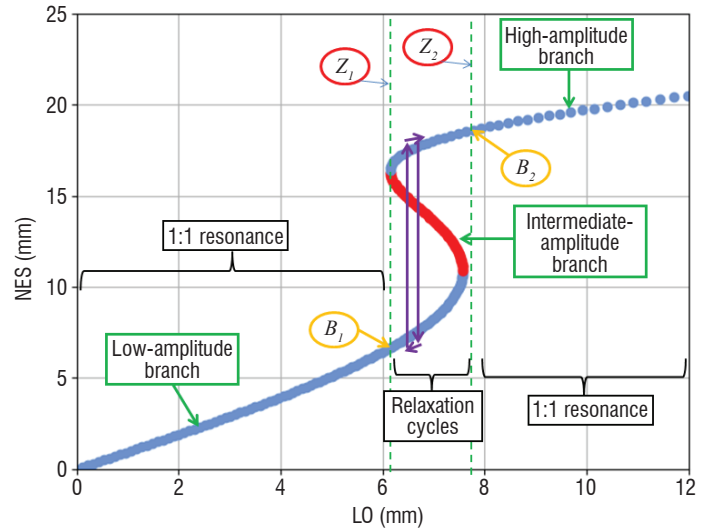


Figure 7 – Invariant manifold (blue circles: stable solutions, red circles: unstable solutions)

An example of an invariant manifold is presented in Figure 7. In this figure, each circle represents a possible solution for the movement. To understand this manifold, let us look at a particular point. For instance, if the periodic amplitude of the LO is 4 mm, then there is only one corresponding amplitude at 4.1 mm for the NES.

In the whole plot, solutions can be grouped into three distinct branches, depending on the NES amplitude: the low-amplitude branch (blue), the intermediate-amplitude branch (red) and the high-amplitude branch (blue). For a movement of the LO below 6.2 mm, only one stable branch of solutions exists for  $N_1$  and  $N_2$ . A 1:1 resonance, also called a Constant Response Amplitude (CAR), can be observed: the NES has almost the same amplitude as the LO, but with a phase difference of 180°. In this zone, the NES is inactive because it only follows the LO movement.

Between 6.2 and 7.6 mm, a first bifurcation point  $B_1$  is reached. In this zone, there are three solution branches: two stable ones on either side of an unstable one. These three solutions are differentiated by the NES amplitude: the low-amplitude one and the high-amplitude one for stable solutions, and the intermediate-amplitude one for the unstable solution. This particular configuration is called a "cusp catastrophe" in nonlinear dynamics literature ([23], [10]) and is at the origin of a special movement called "relaxation cycles", which can be observed both numerically and experimentally. For one value of the LO amplitude, the system is first attracted by a low-amplitude solution of the NES, but fast jumped to the high-amplitude branch. Being on this branch, the NES dissipates much more energy through viscous damping  $c_2$ . Thus, the whole system loses energy and jumps back to a low-amplitude solution. Of course, being back on this branch, the system receives vibratory energy again and its amplitude increases, until its jump to the high-amplitude solution is repeated. This strange behavior is due to the presence of an unstable solution, which makes the jumps appear constantly. This phenomenon, also called a Strongly Modulated Response (SMR), will be illustrated in the following by experimental tests.

Above 7.6 mm, a second bifurcation point  $B_2$  is crossed: there is again a single stable solution for the LO-NES couple. It is characterized by a very high magnification of the NES compared to the LO, and then by a high dissipation of energy by the NES. However, contrary to the previous zone, here the dynamical system is simply locked in a 1:1 resonance (CAR).

As displayed in Figure 7, the invariant manifold has three zones that are delimited by two points of inflexion. These points can be analytically computed by deriving the invariant manifold expression and equating the resulting equation to zero

$$Z_1 = \frac{9}{4K} \left( 2 - \sqrt{1 - 3\lambda_2^2} \right), \quad Z_2 = \frac{9}{4K} \left( 2 + \sqrt{1 + 3\lambda_2^2} \right) \quad [23]$$

With  $Z = N_{20}^2$ . Two remarks should be made on these points. First, they both depend on the cubic stiffness coefficient  $K$  and on the NES damping  $\lambda_2$ . From  $Z_1$ , a condition of existence for relaxation cycles is  $\lambda_2 < 1/\sqrt{3}$ . It means that the NES damping should not be higher

than this threshold; otherwise, no energetic relaxation cycles could appear.

Secondly, the NES activation threshold depends on the inverse of the cubic stiffness coefficient  $K$ . Thus, a low threshold would be obtained for a high value of  $K$ , which implies a high value of the spring stiffness coefficient  $k$ . Therefore, contrary to common sense when looking at Figure 3, it is better to select very stiff springs when a high NES amplitude is sought. In fact, softer springs would not be able to create strongly nonlinear dynamics, and thus achieve efficient vibration mitigation.

After having presented the analytical model and the mathematical methods that gave approximated solutions, all inputs are now gathered to analyze data coming from the experimental demonstrator (Figure 3). As a reminder, the natural frequency of LO is 5.05 Hz. Swept-sine tests were performed between 4 and 6 Hz at a slow rate of 0.05 oct/min and at 7 levels of force, regularly spaced between 17.2 and 23.1 N. The response of the LO is shown in Figure 8. Two kinds of response can be observed. As long as the LO movement has not reached a certain amplitude level, it behaves like a classical linear oscillator. Once this threshold is exceeded, relaxation cycles appear (see Figure 9). They are characterized by a strong irreversible transfer

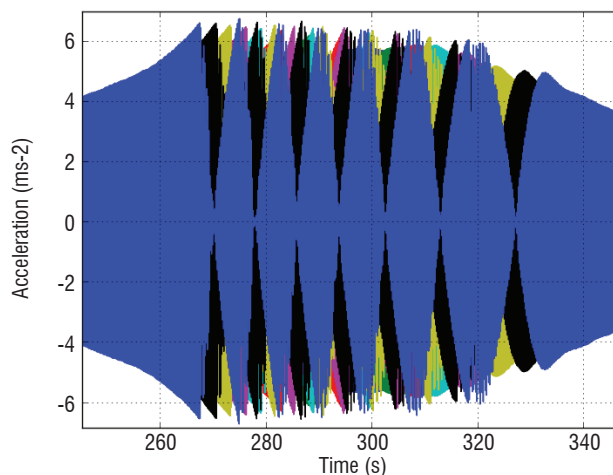


Figure 9 – Zoom on relaxation cycles

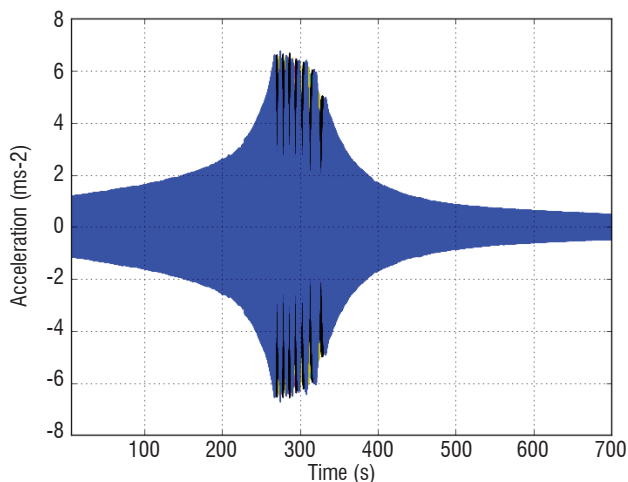


Figure 8 – Response of the LO in the temporal domain

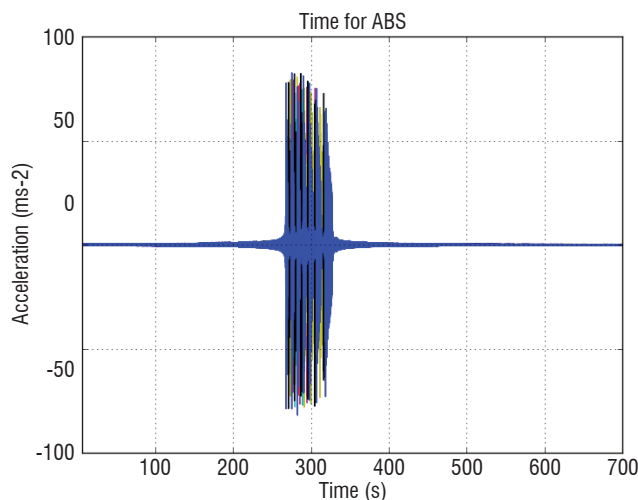


Figure 10 – Response of the NES

Caption for the three figures: 7 curves for 7 levels of force (17.2 to 23.1 N), sweep-sines from 4 to 6 Hz, sweep rate of 0.05 oct/min

of energy between the LO and the NES. Consequently, we can see in Figure 10 that the NES moves significantly only when these cycles are activated. Outside this regime, the NES movement only follows the LO oscillations: therefore it can be considered as inactive.

The LO and NES spectra are also instructive. The NES prevents the structure from exceeding a certain level of vibration (Figure 11 and Figure 12). The more the excitation force increases, the more broadband the frequency range is, since relaxation cycles are increasingly

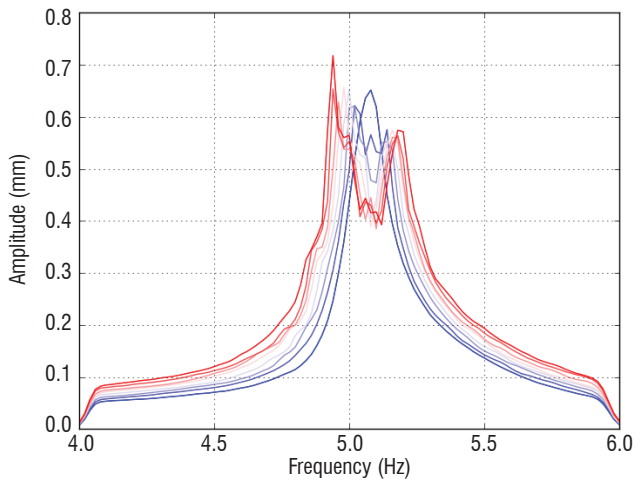


Figure 11 – LO spectra

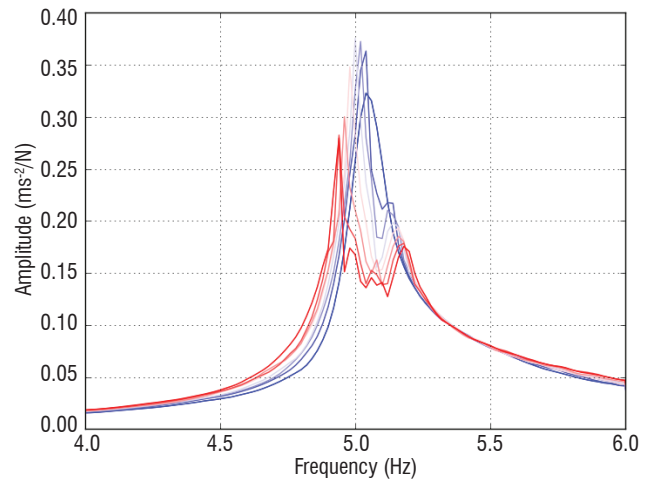


Figure 14 – LO FRFs

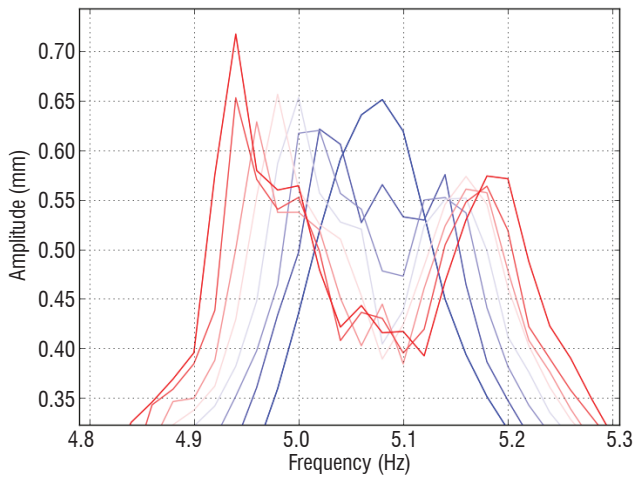


Figure 12 – Zoom on the primary structure spectra

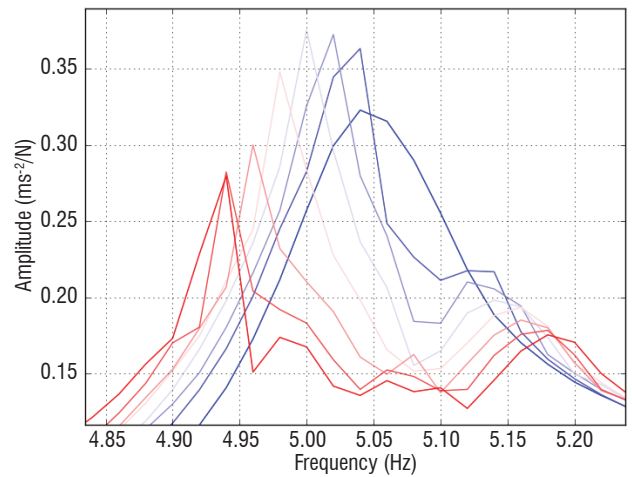


Figure 15 – Zoom on FRFs

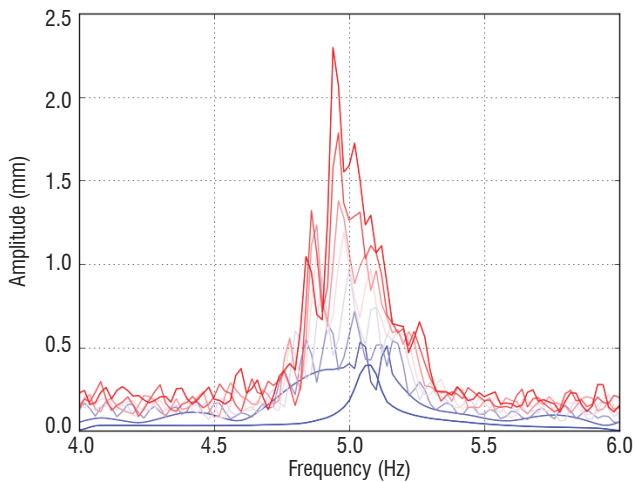


Figure 13 – NES spectra

Caption for the three figures: 7 curves for 7 levels of force, from dark blue (17.2 N) to dark red (23.1 N)

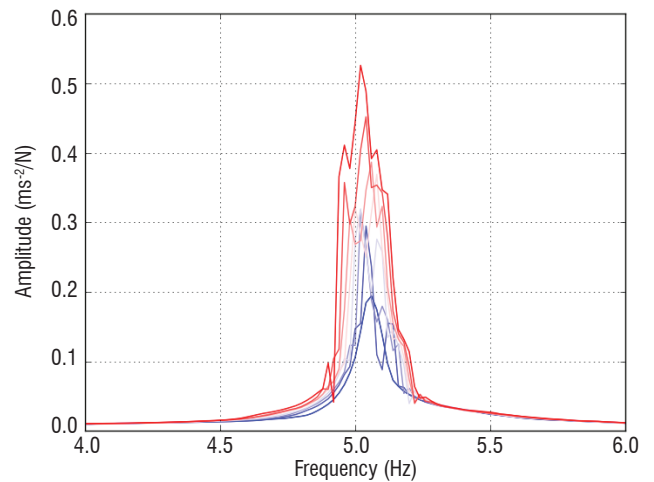


Figure 16 – NES FRFs

Caption for the three figures: 7 curves for 7 levels of force, from dark blue (17.2 N) to dark red (23.1 N)

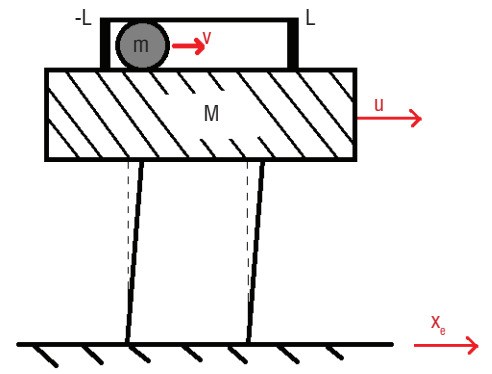
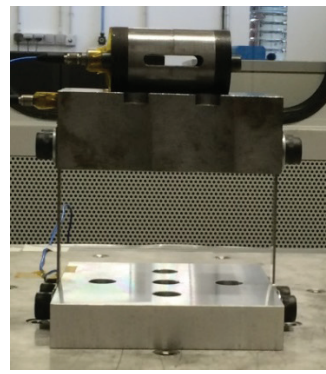
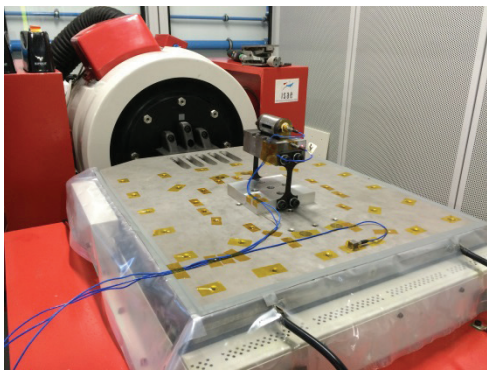


Figure 17 – LO coupled to a VI-NES: the system placed on the vibrating table (left), the LO and VI-NES (center) and its schematic diagram (right)

present. This clearly demonstrates that the efficiency frequency range does not depend on the excitation frequency (at least not on the first order), but rather on the level of excitation. The NES spectra are very disturbed, and it is difficult to interpret them (see Figure 13). It can only be noticed that, when the NES is active, its amplitude level increases as a function of the force level.

Strictly speaking, Frequency Response Functions (FRFs) are not appropriate tools for studying highly nonlinear systems [28]. In any case, they can still be useful to qualify the deviation of a system from a classical linear one. FRFs are computed by taking the cell force as a reference. FRFs of LO are presented in Figure 14. The FRF at the lowest level can easily be found (dark blue curve): it is the only smooth one and there are no relaxation cycles. Indeed, since relaxation cycles are a manifestation of a highly nonlinear behavior, the spectral content during these cycles is very rich. It affects FRFs and gives them a noisy appearance. Furthermore, when the force level was increased, two peaks appeared instead of one, as if the FRFs were cut at their summits (Figure 15). The FRFs of the NES clearly show that this resonance phenomenon suppression is due to the activation of the NES (Figure 16).

### Experimental case No. 2: the Vibro-Impact NES (VI-NES)

The experimental study has been conducted with the aim of observing the behavior of the system and of exploring the different types

of response that the system can exhibit. The relationship between the regimes and the external forcing, in terms of magnitude and frequency, is of particular interest.

The experimental setup is shown in Figure 17 and comprises a primary single-degree-of-freedom linear oscillator (LO), to which the VI-NES is attached. The LO is harmonically forced by an electrodynamic shaker.

The system is forced by a swept-sine external force with constant amplitude and the primary mass displacement is measured by means of a Laser Doppler Vibrometer.

$f_0$ [Hz]	$K$ [N/m]	$C$ [N/ms]	$\xi$ [%]	$M$ [kg]	$m$ [kg]	$\varepsilon = m / M$ [%]
21.18	67421	8.566	0.8	3.807	0.032	0.84

Figure 18: Modal parameters of the primary system and mass value of the primary system  $M$ , of the VI-NES  $m$  and their ratio  $\varepsilon$

The modal parameters of the LO and the mass values are shown in Figure 18. It is important to notice the very small mass ratio between the VI-NES and the primary system, *i.e.*, less than 1%.

Figure 19 (left) shows the displacement spectra for the system with and without VI-NES. We can observe that two types of qualitatively different responses exist when the VI-NES is active and, depending on the magnitude and the frequency of the external forcing, either one or the other may appear.

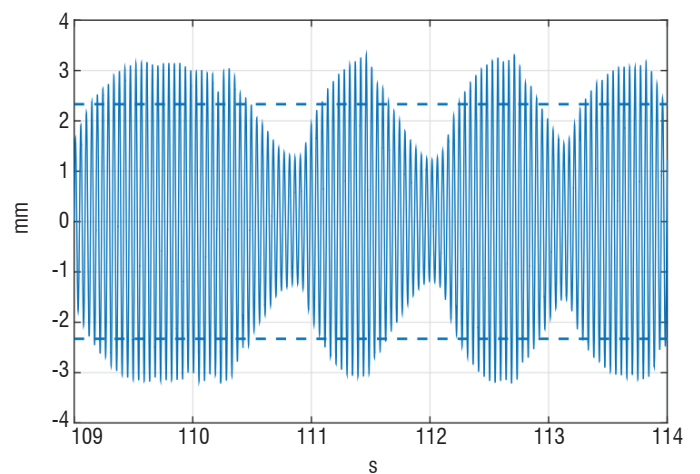
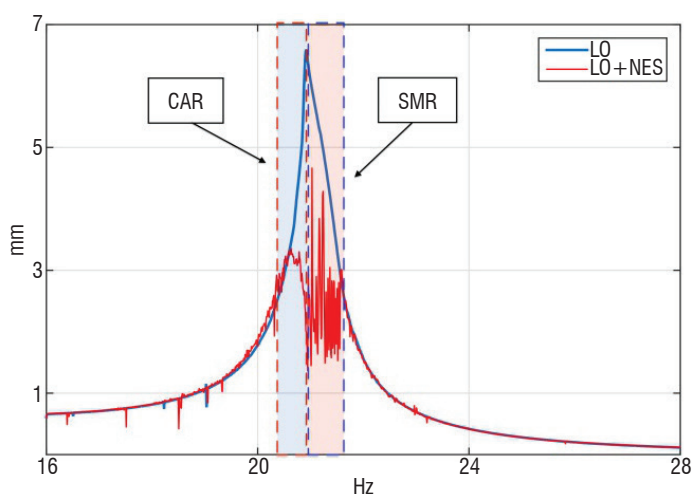


Figure 19 – Left: experimental spectra of the primary mass displacement with (red) and without (blue) the VI-NES. Right: recorded time signal of a SMR, the dashed lines indicate the amplitude of the LO without the VI-NES under the same forcing conditions.



We can classify the responses as:

- Strongly Modulated Response (SMR): the primary system goes through alternatively increasing and decreasing amplitude cycles and then the fast oscillations appear to be modulated. This behavior is caused by a repeated activation/deactivation of the VI-NES (Figure 19 right).
- Constant Amplitude Response (CAR): the VI-NES is stably active and the amplitude of the primary mass displacement remains constant.

The VI-NES seems to accomplish its task as a vibration absorber well, since the response amplitude is reduced near the resonance of the primary system. This is the proof that a Targeted Energy Transfer occurs from the LO towards the VI-NES and that the energy is dissipated by the impacts. It is important to emphasize that this goal has been achieved, despite a proper sizing process not having been carried out and with a significantly small mass ratio  $\varepsilon = 0.84\%$ . This result proves that the VI-NES is able to automatically tune itself to the primary system. This is a relevant general feature of nonlinear absorbers caused by the absence of a natural frequency for these devices.

By looking at the spectrum in Figure 19, one can draw the conclusion that a criterion exists on the primary mass displacement to activate the VI-NES. In fact, an amplitude/energy threshold is observed, beyond which the VI-NES is active.

The schematic diagram of the model is presented in Figure 17 (right). We define the variables  $u$ ,  $v$  and  $x_e$  as the displacements of the primary mass  $M$ , of the NES mass  $m$  and of the base, respectively. We model the shocks as instantaneous impacts by using the basic concepts of Newtonian mechanics:

$$\begin{aligned} \dot{u}(t_j^+) - \dot{v}(t_j^+) &= -r(\dot{u}(t_j^-) - \dot{v}(t_j^-)) \\ M\dot{u}(t_j^+) + m\dot{v}(t_j^+) &= M\dot{u}(t_j^-) + m\dot{v}(t_j^-) \end{aligned} \quad [24]$$

Where  $t_j^+$  and  $t_j^-$  are the time instants after and before the  $j^{th}$  impact, respectively. The first equation provides a relation for the relative velocity of the two colliding masses after and before the impact, by using the restitution coefficient  $0 < r < 1$ . This allows the impact to be characterized from completely elastic  $r=1$  to completely plastic  $r=0$ .

The second equation expresses the momentum conservation throughout the impact. Then, the motion equations are:

$$\begin{cases} \ddot{u} + 2\omega_0\xi\dot{u} + \omega_0^2u + \frac{m(1+r)}{m+M} \sum_j \dot{w}^- \delta_j^- = \omega_0^2x_e + 2\omega_0\xi\dot{x}_e \\ \varepsilon\ddot{v} - \frac{m(1+r)}{M+m} \sum_j \dot{w}^- \delta_j^- = 0 \end{cases} \quad [25]$$

where  $\omega_0^2 = \frac{K}{M}$  and  $2\omega_0\xi = \lambda/M$ .

The previous system [25] can be studied by means of the Multiple Scales method [26], which allows us to separate the various dynamic behaviors of the problem, happening at different time scales.

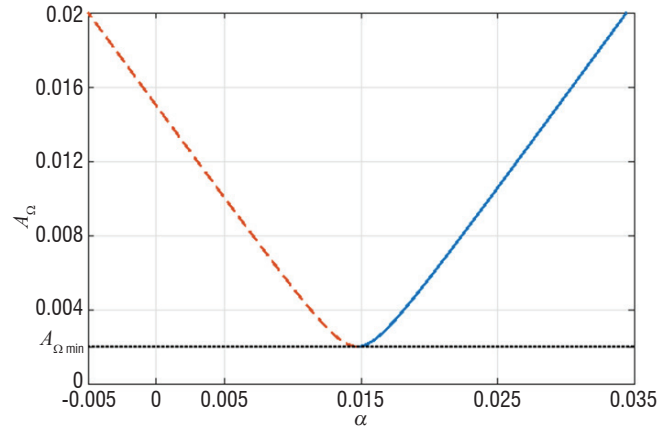


Figure 20 – Slow Invariant Manifold -  $r = 0.65$ ,  $L = 15$  mm

For the sake of conciseness, all mathematical steps are not detailed like in the previous section; they are given in [19]. We directly go to the important result that the analytic study provides us with: the Slow Invariant Manifold (SIM) of the problem, a mathematical tool that gathers all of the possible solutions that the system may exhibit. Under the condition of two impacts per oscillation, the SIM, shown in Figure 20, can be expressed by the following equation, where  $A_\Omega$  and  $\alpha$  are two variables that are strictly related to the displacements  $X$  and  $w$ .

$$\alpha = \frac{L \pm \sqrt{1 + \sigma^2} \sqrt{A_\Omega^2 - A_{\Omega_{min}}^2}}{1 + \sigma^2} \quad [26]$$

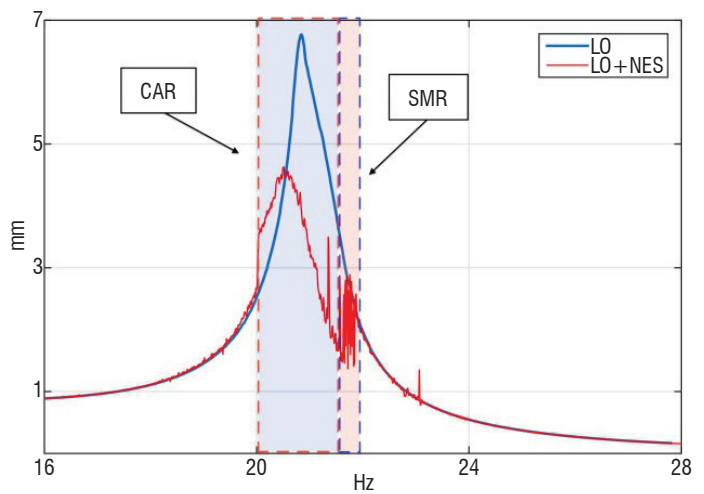
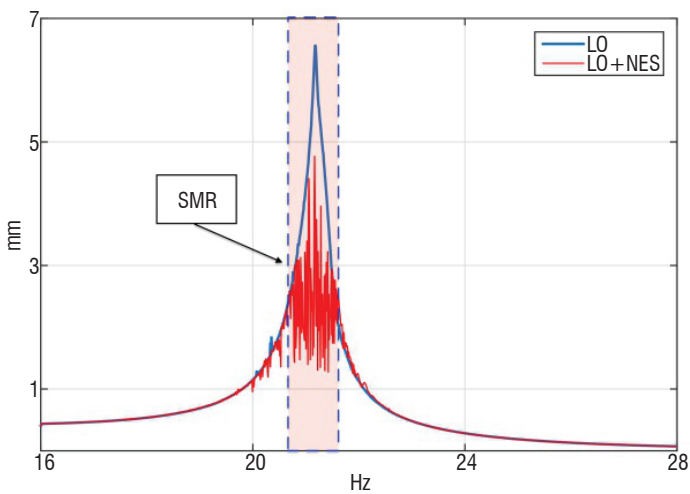


Figure 21 – Spectra of the primary mass displacement with and without VI-NES for  $F = 0.2g$  (left) and  $F = 0.4g$  (right).

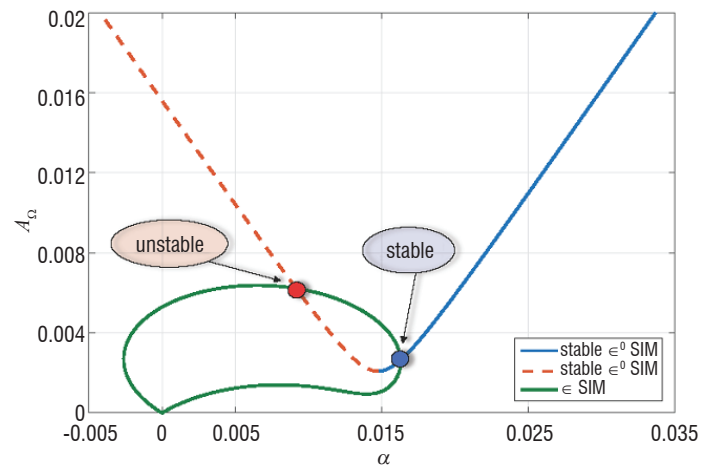
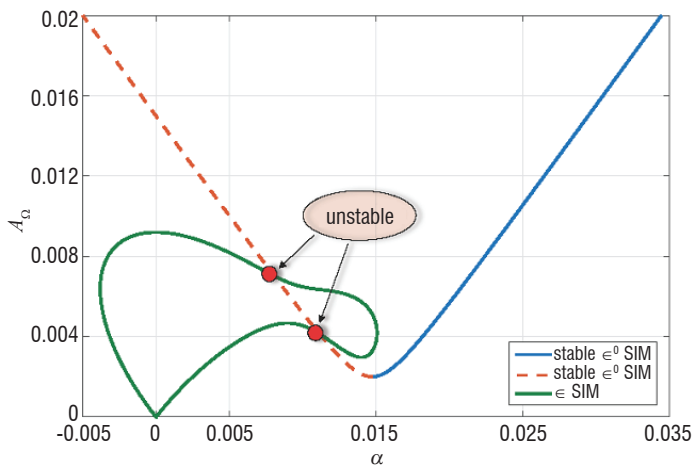


Figure 22 – SIM and fixed points for an external force level of  $F=0.2g$  and  $\Omega = \frac{\omega}{\omega_0} = 1$  (left) and  $F = 0.4g$  and  $\Omega = \frac{\omega}{\omega_0} = 1.02$  (right).

with  $\sigma = \frac{2(1-r)}{\pi(1+r)}$  and where  $A_{\Omega_{min}} = \frac{\sigma L}{\sqrt{1+\sigma^2}}$  is a minimum value of amplitude  $A_{\Omega}$  for solutions to exist.

Some important information that the SIM contains is that a minimum  $A_{\Omega}$  must exist for solutions to appear. This point mathematically represents a saddle-node bifurcation. Starting from this bifurcation point, two solution branches appear: one stable and one unstable.

Once the SIM has been obtained, we can take our analysis further and study the previous system of dynamical equations at the next order. Similarly, we reach an expression relating  $A$  and  $\alpha$  (not reported here for the sake of conciseness), which represents the fixed points of the problem. The intersections between the SIM and the fixed points represent the solutions of the problem.

Figure 21 shows the experimental spectra of the primary mass displacement with and without the VI-NES attached. The two different kinds of regime, constant amplitude and strongly modulated responses (CAR and SMR), have been highlighted. We can see that for  $F=0.2g$ , *i.e.*, for a low level of external force, the only type of response observed is the strongly modulated response, whereas when the external forcing increases, the constant amplitude response appears and the transition from one type of regime to another is a function of the forcing frequency.

Figure 22 shows the SIMs for two different cases of external force amplitude and frequency. For the lower level (Figure 22 left), the only fixed points attainable are unstable points for any frequency  $\Omega$ . The only type of possible response is then the strongly modulated response. This result is in perfect agreement with the experimental observations.

For the higher level of the external force (Figure 22 right) the behavior of the SIMs is different. As  $\Omega$  grows, the system goes from a state of no solution (no impacts) to a state where two fixed points exist: one stable and one unstable. The stable one is reached and the system presents a CAR. When  $\Omega$  increases further, just before the disappearing of solutions, the two intersections of the SIMs are both unstable points. Thus, the system exhibits a SMR. This behavior is also in perfect agreement with the experimental observations in Figure 21.

## Conclusion

In this work, the vibration mitigation based on nonlinear absorbers has been explored. The links and differences between linear and nonlinear absorbers have been discussed. Two experimental cases of NES have been carried out. For each NES, approximated solutions of the nonlinear dynamical equation system were obtained by a combination of the Complexification-Averaging method and the Multiple Scales method. Fixed points of the approximated system were computed and, consequently, the invariant manifold was computed with its stability matrix. It was shown that different regimes could occur, depending on the LO response amplitude. When an amplitude threshold is reached, very energetic solutions appear and the NES is active because it dissipates a significant amount of energy. In conclusion, a NES is able to significantly reduce the level of vibrations, and even to suppress the resonance peak phenomenon, for a very small mass ratio below 1%. Furthermore, it can be active over a wide frequency range, since its behavior mainly depends on the amplitude level of the LO. It is believed by the authors that the NES can be an effective solution for vibration mitigation, especially for aircraft embedded equipment. In the future, several technologies could be explored and adapted to industrial applications ■

## Nomenclature and Acronyms

$x$	Displacement at one location of a structure
$\dot{x}$	Velocity at one location of the structure
$\ddot{x}$	Acceleration at one location of a structure
NES	(Nonlinear Energy Sink)
LO	(Linear Oscillator)
TMD	(Tuned Mass Damper)
DVA	(Dynamical Vibration Absorber)
FRF	(Frequency Response Function)
SMR	(Strongly Modulated Response)
CAR	(Constant Amplitude Response)
SIM	(Slow Invariant Manifold)

## References

- [1] F. R. ARNOLD - *Steady-State Behavior of Systems Provided with Nonlinear Dynamic Vibration Absorbers*. Journal of Applied Mechanics, 22, pp.487-492, 1955.
- [2] T. ASAMI, O. NISHIHARA, A. M. BAZ - *Analytical Solutions to H1 and H2 Optimization of Dynamic Vibration Absorbers Attached to Damped Linear Systems*. Journal of Vibration and Acoustics, 124, pp.284-295, 2002.
- [3] S. BENACCHIO, A. MALHER, J. BOISSON, C. TOUZE - *Design of a Magnetic Vibration Absorber with Tunable Stiffnesses*. Nonlinear Dynamics, 85, pp.893-911, 2016.
- [4] S. B. CHOI, W. K. KIM - *Vibration Control of a Semi-Active Suspension Featuring Electrorheological Fluid Dampers*. Journal of Sound and Vibration, 234, pp.537-546, 2000.
- [5] J. P. DEN HARTOG - *Mechanical Vibrations*. Dover Books on Engineering, 4<sup>th</sup> edition, 1985.
- [6] S. J. DYKE, B. F. SPENCER, M. K. SAIN, J. D. CARLSON - *Modeling and Control of Magnetorheological Dampers for Seismic Response Reduction*. Smart Materials and Structures, 5, pp.565-575, 1996.
- [7] H. FRAHM - *A Device for Damping Vibrations of Bodies*. 1911.
- [8] Y. FUJINO, M. ABE - *Design Formulas for Tuned Mass Dampers Based on a Perturbation Technique*. Earthquake Engineering and Structural Dynamics, 22, pp.833-854, 1993.
- [9] O. V. GENDELMAN - *Transition of Energy to a Nonlinear Localized Mode in a Highly Asymmetric System of Two Oscillators*. Nonlinear Dynamics, 25, pp.237-253, 2001.
- [10] J. GUCKENHEIMER, P. HOLMES - *Nonlinear Oscillations, Dynamical Systems, and Bifurcations of Vector Fields*. vol. 42, Springer-Verlag New York, 1983.
- [11] G. HABIB, T. DETROUX, R. VIGUIE, G. KERSCHEN - *Nonlinear Generalization of Den Hartog's Equal Peak Method*. Mechanical Systems and Signal Processing, vol. 52-53, pp.17-28, 2015.
- [12] J. B. HUNT, J. C. NISSEN - *The Broadband Dynamic Vibration Absorber*. Journal of Sound and Vibration, 83, pp.573-578, 1982.
- [13] I. N. JORDANOV, B. I. CHESHANKOV - *Optimal Design of Linear and Nonlinear Dynamical Vibration Absorbers*. Journal of Sound and Vibration, 123, pp.157-170, 1988.
- [14] I. N. JORDANOV, B. I. CHESHANKOV - *Optimal Design of Linear and Nonlinear Dynamical Vibration Absorbers, Reply*. Journal of Sound and Vibration, 132, pp.157-159, 1989.
- [15] B. P. MANN, B. A. OWENS - *Investigations of a Nonlinear Energy Harvester with a Bistable Potential Well*. Journal of Sound and Vibration, vol.329, pp.1215-1226, 2010.
- [16] B. C. NAKRA - *Vibration Control in Machines and Structures Using Viscoelastic Damping*. Journal of Sound and Vibration, 211, pp.449-465, 1998.
- [17] J. ORMONDROYD, J. P. DEN HARTOG - *The Theory of the Dynamical Vibration Absorber*. ASME Journal of Applied Mechanics, 50(7), pp.9-22, 1928.
- [18] E. PENNESTRI - *An Application of Chebyshev's Min-Max Criterion to the Optimal Design of a Damped Dynamic Vibration Absorber*. Journal of Sound and Vibration, 217, pp.757-765, 1998.
- [19] G. PENNISI, C. STEPHAN, E. GOURC, G. MICHON - *Experimental Investigation and Analytical Description of a Vibro-impact NES Coupled to a Single-Degree-of-Freedom Linear Oscillator Harmonically Forced*. Nonlinear Dynamics, vol.88, pp.1769-1784, 2017.
- [20] L. A. PIPES - *Analysis of a Nonlinear Dynamic Vibration Absorber*. Journal of Applied Mechanics, 20, pp.515-518, 1953.
- [21] A. PREUMONT - *Vibration Control of Active Structures 3<sup>rd</sup> Edition*. Springer, 2011.
- [22] R. E. ROBERSON - *Synthesis of a Nonlinear Dynamic Vibration Absorber*. Journal of the Franklin Institute, 254, pp.205-220, 1952.
- [23] R. THOM - *Structural Stability and Morphogenesis: An Outline of a General Theory of Models*. Reading, MA: Addison-Wesley, 1989.
- [24] A. THOMPSON - *Auxiliary Mass Throw in a Tuned and Damped Vibration Absorber*. Journal of Sound and Vibration, 70, pp.481-486, 1980.
- [25] A. THOMPSON - *Optimum Tuning and Damping of a Dynamic Vibration Absorber Applied to a Force Excited and Damped Primary System*. Journal of Sound and Vibration, 77(3), 1981.
- [26] A. F. VAKAKIS, O. V. GENDELMAN, L. A. BERGMAN, D. M. MCFARLAND, G. KERSCHEN, Y. S. LEE - *Nonlinear Targeted Energy Transfer in Mechanical and Structural Systems I*. Springer, New York, 2008.

- [27] A. F. VAKAKIS, O. V. GENDELMAN, L. A. BERGMAN, D. M. MCFARLAND, G. KERSCHEN, Y. S. LEE - *Nonlinear Targeted Energy Transfer in Mechanical and Structural Systems II*. Springer, New York, 2008.
- [28] K. WORDEN, G. R. TOMLINSON - *Nonlinearity in Structural Dynamics: Detection, Identification and Modelling*. CRC Press, 2000.

## AUTHORS



**Cyrille Stephan** After having graduated from the ENSMM (*École Nationale Supérieure en Mécanique et Microtechniques*) in 2004, Cyrille Stephan obtained his PhD in Sciences for Engineering at the University of Franche-Comté in 2009. He then joined ONERA and is currently in charge of developing methods for structural dynamics, especially for signal processing and nonlinear dynamics.



**Guilhem Michon** Having graduated from INSA Lyon in 2002, Guilhem Michon obtained a PhD from the University of Lyon in 2006. Since 2007, he has been a Professor at ISAE-Supaero, conducting his research in nonlinear dynamics at the Clément Ader Institute (UMR CNRS 5312).



**Giuseppe Pennisi** Having graduated in 2012 with a MS in Aerospace Engineering from the *Politecnico di Milano* and a MS in Aerospace Engineering from the *Institut Supérieur de l'Aéronautique et de l'Espace* (ISAE) in Toulouse, Giuseppe Pennisi obtained his PhD in Mechanical Engineering in 2016, working within the context of a collaboration between ONERA and ISAE. He then joined ENSTA ParisTech as a Postdoctoral Researcher. Dynamics and Control, Vibrations, and Nonlinear Dynamics are among his main research interests.